Far-IR magnetospectroscopy of magnons and electromagnons in TbFeO_{3} single crystals at low temperatures

T. N. Stanislavchuk, Yazhong Wang, S.-W. Cheong, and A. A. Sirenko

Phys. Rev. B **95**, 054427 — Published 21 February 2017

DOI: 10.1103/PhysRevB.95.054427

Far-IR magnetospectroscopy of magnons and electromagnons in $TbFeO_3$ single crystals at low temperatures

T. N. Stanislavchuk*,[1] Yazhong Wang,[2] S.-W. Cheong,[2] and A. A. Sirenko[1]

[1] *Department of Physics, New Jersey Institute of Technology, Newark, New Jersey 07102, USA*

[2] *Rutgers Center for Emergent Materials and Department of Physics and Astronomy, Rutgers University, Piscataway, New Jersey 08854, USA*

Abstract

Transmittance spectra of $TbFeO_3$ single crystals have been studied in the far infrared spectral range 15 − 120 cm^{-1} in the external magnetic fields up to 9 T and at low temperatures down to 1.5 K. The temperature and magnetic-field dependencies of the antiferromagnetic resonance (AFMR) modes have been measured below and above the magnetic ordering temperature of Tb moments $T_N^{Tb} = 3.3\,K$. Both the quasi-ferromagnetic and quasi-antiferromagnetic modes of AFMR demonstrate hardening at $T < T_N^{Tb}$. The quasi-antiferromagnetic mode gains electric-dipole activity along the *c*-axis below T_N^{Tb} and thus behaves as a hybrid, *i.e.*, both electric- and magnetic-dipole active, mode. In addition to AFMR modes, below T_N^{Tb} we observed appearance of electromagnon excitation at about 27 cm^{-1}, which is electric-dipole active along the *c*-axis. The electromagnon is optically active only in a narrow temperature range $2.7\,K < T < T_N^{Tb}$ at H=0 and in a narrow range of magnetic fields 2.4 − 2.7 T applied along the *b*-axis at T=1.5 K. We argue that this electromagnon appears in magnetic phases, which are compatible with a spontaneous electric polarization along the b-axis.

PACS: 75.85.+t, 75.30.Ds, 78.20.Ls, 78.30.-j

---

* Author to whom correspondence should be addressed. Electronic mail: stantar@njit.edu

I. INTRODUCTION

$TbFeO_3$ has an orthorhombic perovskite structure that belongs to the D_{2h}^{16} ($Pbnm$) space group with four $TbFeO_3$ molecules per unit cell [1,2]. The Fe^{3+}–Fe^{3+} exchange interaction leads to an antiferromagnetic (AFM) ordering of the Fe subsystem at a high transition temperature of $T_N(\mathrm{Fe}) \approx 650$ K [3]. The resulted spin structure is $\Gamma_4(G_xF_z)$ where the *G*-type antiferromagnetic order along the *a* orthorhombic axis appears due to a negative symmetric superexchange interaction and *F*-type ferromagnetic canting along the *c* orthorhombic axis - due to an antisymmetric Fe^{3+}–Fe^{3+} super-exchange (Dzyaloshinskii-Moriya) interaction. At high temperatures Tb subsystem is paramagnetic and can be polarized along two Ising axes within the *ab* plane at the angle $\alpha = \pm 36^\circ$ from *a* by the Tb-Fe interaction when the antiferromagnetic vector *G* of Fe spins leaves the *ab* plane [4]. This leads to a spin-reorientation transition with the onset at T_{SR1}≈8.5 K below which Fe spins continuously rotate in the *a*–*c* plane so that their structure changes from $\Gamma_4(G_xF_z)$ to $\Gamma_2(G_zF_x)$ while Tb moments become polarized in the *ab* plane according to $\Gamma_2(f_xc_y)$ state [5,6]. With further temperature decrease the Tb–Tb interaction leads to an antiferromagnetic ordering of Tb moments [7]. It was shown [4,8] that this transition occurs in two stages: at T_N^{Tb}=3.3 K Tb moments antiferromagnetically order into intermediate $\Gamma_{82}(a_xg_yf_xc_y)$ phase which at $T_{SR2} \approx 3.1\,\mathrm{K}$ causes a reverse spin reorientation transition of Fe spins $\Gamma_2(G_zF_x) \rightarrow \Gamma_4(G_xF_z)$ with simultaneous reorientation of Tb spins into purely antiferromagnetic $\Gamma_8(a_xg_y)$ phase.

It is also known that the external magnetic field *H* applied along *a*, *b*, and *c* axes results in an additional spin reorientation (SR) transitions that have been studied at low temperatures using magnetization methods [9,10,11,12], Mössbauer spectroscopy [11], neutron diffraction [13], magnetostriction [14] and sound velocity [8] measurements. Several anomalies have been found including the two-stage metamagnetic transitions for $H \| b$ at $T < T_N^{Tb}$. The *H*-*T* phase diagram for $TbFeO_3$ is not complete yet and this compound continues to reveal its nontrivial magnetic properties. For example, an unusual magnetic state of the ordered Tb^{3+} spins with a long incommensurate period of several hundred nm has been recently found in $TbFeO_3$ upon application of an external magnetic field $H \| c$ [13].

Spectra of magnetic excitations provide important information about nontrivial rare earth–iron R^{3+}–Fe^{3+} interaction in $RFeO_3$ compounds (*R*=rare earth) especially if measured in proximity to the phase transitions that change the spin structure. Magnons in $TbFeO_3$ have been previously studied using inelastic neutrons [15], Raman scattering [16,17] and submillimeter backward-wave oscillator spectroscopy [18]. Related $RFeO_3$ (*R*=Yb, Tm, Er, Dy, and Ho) compounds have been studied using neutron scattering [19], Raman [16,17,20,21], far-IR [22,23] and submillimeter [18,24] spectroscopies and ultrafast laser pulses [25]. All experiments agree with the theoretical prediction for existence of two magnon modes, namely quasi-ferromagnetic

(q-FM) and quasi-antiferromagnetic (q-AFM) modes of AFM resonance (AFMR), which appear in a simplified model of two Fe sublattices with four ions in the orthorhombic primitive cell. The frequencies of the q-FM and q-AFM modes at $\vec{q} = 0$ and T=5 K are reported to be at 11.8 and 18.5 cm^{-1}, respectively, at room temperature and gradually increase to 18 and 23 cm^{-1}, respectively, at T=5 K [16,17]. In a more precise model, which takes into consideration the R^{3+} spins, the number of magnons in RFeO$_3$ should increase up to four. Two additional magnons that appear due to R^{3+} spins are predicted to have relatively low frequency, which should be less than 5 cm^{-1} at $\vec{q} = 0$. These modes, which are expected to be the most sensitive to Tb^{3+}–Tb^{3+} interaction are difficult for optical observation and, unfortunately, are falling far below our experimental spectral range. Nevertheless, temperature and magnetic field dependencies of the Fe-related q-FM and q-AFM modes should reflect important details of nontrivial Tb^{3+}–Fe^{3+} interaction. For example the earlier Raman scattering measurements of TbFeO$_3$ already indicated the stiffening of q-AFM mode due to the strong exchange coupling between the Fe and Tb spins [16].

While the properties of magnetic excitations in TbFeO$_3$ have been studied in literature at T > 4.2 K, there are no experimental data for magnons' behavior below the temperature of Tb antiferromagnetic ordering T_N^{Tb}=3.3 K and in the external magnetic fields. This temperature region in RFeO$_3$ orthoferrites is of special interest because the R^{3+} ions order according to one of the Γ_i (i=5–8) irreducible representations, which are not compatible with inversion symmetry and thus allow for a linear magnetoelectric effect. As a result, one can also expect existence of a dynamic magnetoelectric effect manifested as an appearance of electric-dipole active magnetic excitations, *i.e.* electromagnons. The possibility of entanglement between electric-dipole and magnetic-dipole oscillations was demonstrated for the first time in theoretical works of V. G. Bar'yakhtar and I. E. Chupis at the end of 1960's [26] but it was not before 2006 that electromagnons were experimentally observed in the THz spectral region of TbMnO$_3$ and GdMnO$_3$ crystals [27]. Since then electromagnons have been observed in many magnetic compounds, review of which can be found in Refs. [28, 29, 30]. The current interest to electromagnons is due to their non-trivial optical properties, such as directional dichroism [31, 32] and giant optical activity [33], and promising new functionalities, such as magnetically controlled directional light switches [34] and control of magnetism on a sub-picosecond time scale [35]. The main microscopic mechanisms driving electric dipole-activity of magnetic excitations are considered to be symmetric exchange striction [36], antisymmetric exchange interaction in the frame of a spin-current model [37] and spin-dependent p–d hybridization [38]. While all these mechanisms originate from those governing magnetically induced ferroelectricity [39, 40, 41, 42, 43], in a given compound the particular mechanisms driving static and dynamic magnetoelectric effects do not necessarily coincide. For example, the electromagnon activity in TbMnO$_3$ crystal arises from symmetric exchange striction [36], but the ferroelectric polarization is due to antisymmetric exchange interaction [40, 44]. For this reason, the emergence of electromagnons is also possible in non-multiferroic states, when the mechanism driving electric-

dipole activity of magnetic excitations does not produce ferroelectric polarization. This scenario is realized, for example, in $Ba_2Mg_2Fe_{12}O_{22}$, where an electromagnon was reported despite the absence of spontaneous electric polarization in a zero magnetic field [45].

The existence of electromagnons in RFeO$_3$ orthoferrites was theoretically predicted back in 1980 in Ref. [46] and has been recently confirmed for DyFeO$_3$ where, in addition to two magnetic-dipole-active AFMR modes, two electromagnon modes appear at 20 and 50 cm^{-1} at temperatures below $T_N^{Dy} = 4.2$ K and are electric-dipole-active along the *c*-axis [22]. The purpose of this paper is to study magnetic excitations in TbFeO$_3$ single crystal in the vicinity of phase transitions at temperatures down to 1.5 K and in strong magnetic fields up to 9 T applied along the three main crystallographic directions: *a*, *b* and *c*. We will also compare the low-temperature magnon and electromagnon spectra between the two related compounds: TbFeO$_3$ and recently studied DyFeO$_3$ [22].

II. EXPERIMENT

The bulk crystals of TbFeO$_3$ were grown by the floating zone technique in the form of long rods. The lattice parameters and orientation of the measured single crystals were determined at room temperature using X-ray diffraction. The following lattice parameters were found: *a*=0.53287 nm, *b*=0.55994 nm, *c*=0.76397 nm. Samples were cut and mechanically polished in a form of platelets oriented along the orthorhombic *a*, *b*, and *c* directions. The in-plane areas were about 6 × 6 mm^2. The sample thickness of about 0.3 mm was chosen for transmission measurements. To reduce the interference fringes in optical spectra, the opposite sides of the samples were wedged at an angle of about 5 deg. The far-infrared optical experiments were carried out at the National Synchrotron Light Source (NSLS), Brookhaven National Laboratory, at the U4IR beamline using a Bruker i66v IR spectrometer coupled to an optical Oxford SM4000 superconducting magnet and a LHe-pumped (~1.6 K) bolometer. Transmittance spectra were measured with a spectral resolution of 0.3 cm^{-1} in the spectral range between 15 and 120 cm^{-1} at temperatures 1.5-50 K and in external magnetic fields up to 9 T applied in the Faraday configuration, so that the directions of the external magnetic field and the light propagation coincided, while the electric $\vec{e}$ and magnetic $\vec{h}$ fields of light were always perpendicular to the external magnetic field. In the text below we will use the notation of transmission geometry where a sub-index of the electric or magnetic fields of light will indicate its direction with respect to crystallographic axes. For example, $e_a h_b$ configuration means here that electric field of light $\vec{e}$ is along the *a*-axis, magnetic field of light $\vec{h}$ is along the *b*-axis, and the direction of light propagation and external magnetic field (if any) are both along the missing third index: the *c*-axis. The raw data of transmittance spectra were normalized to transmission through an empty aperture with a size equal to that of the sample. For samples with strong thickness interference fringes we normalized the transmitted intensity to that measured at high temperature or high magnetic fields, where no magnons were present.

III. EXPERIMENTAL RESULTS

In this Section we will discuss temperature and magnetic field dependencies of transmittance spectra of $TbFeO_3$ in the far-infrared spectral range in several complementary experimental configurations. Spectra of magnons were interpreted by means of selection rules for magnetic dipole excitation of q-FM and q-AFM modes in a *Pbnm* structure of orthoferrites [18,47], which are summarized in Table I. We will commence with the temperature behavior of the magnons at H=0 and proceed with their magnetic field dependencies for direction of magnetic field along three crystallographic axes: *a*, *b*, and *c*. At temperatures above $T_N^{Tb} \approx 3.3$ K, we observed the q-AFM and q-FM modes in configurations according to selection rules shown in Table I. At lower temperatures $T < T_N^{Tb}$, the ordering of Tb moments changes the selection rules of Table I so that the q-FM and q-AFM modes can be observed simultaneously in some configurations.

3.1 Magnon spectra at zero magnetic field.

Figure 1 shows temperature dependence of transmittance spectra in the $e_c h_a$ configuration for the temperature range between 2.2 and 25 K. Above T_{SR1}=8.5 K, when Fe spins are in Γ_4 state, one absorption line, which is excited by $h||a$ is observed at ~17.5 cm^{-1}. According to the selection rules from Table I, we attribute this line to the q-FM mode, which is in good agreement with the Raman data in Ref. [17].

At $T_N^{Tb} < T < T_{SR1}$, Fe spins rotate from the Γ_4 configuration to Γ_2. In the Γ_2 phase the q-FM mode can be excited by $h||(b,c)$ and thus cannot be observed in Fig. 1 in this temperature range. Instead, the q-AFM mode becomes active for $h||a$ and appears at ≈22 cm^{-1} in Fig. 1. We note that intensity of the q-FM mode gradually decreases as the temperature approaches T_{SR1} from the above.

Magnetic ordering of Tb moments below T_N^{Tb} leads to hardening of q-FM and q-AFM modes [see Fig. 1(c)]. Also both AFMR modes are now observed simultaneously in the $e_c h_a$ configuration below T_N^{Tb}. In a two sublattice model the AFMR modes are always observed in the complementary configurations (see Table I). Thus magnetic ordering of Tb moments changes the selection rules described in Table I. In addition to the AFMR modes a new broader spectral line appears at ≈ 27 cm^{-1} in a narrow temperature range $3.1\,\mathrm{K} < T < 3.3\,\mathrm{K} = T_N^{Tb}$. This range correlates with the intermediate Γ_{82} phase of Tb moments in the sequence of the Tb magnetic ordering phases [4]. In this case, the temperature of 3.1 K, at which the line at 27 cm^{-1} vanishes from the spectra, corresponds to transition temperature T_{SR2} when Tb moments reorient from $\Gamma_{82}(a_x g_y f_x c_y)$ phase into a purely AFM $\Gamma_8(a_x g_y)$ phase, while Fe spins reorient from the Γ_2 phase back to the high temperature Γ_4 one.

Figure 2 shows temperature dependence of AFMR modes' spectra measured in the $e_b h_a$ configuration. At $T_N^{Tb} < T < 4$ K Fe spins are in the Γ_2 phase and, thus, the q-AFM mode is $h||a$ active and is observed in Fig. 2 at 23 cm^{-1}, similar to what was shown in Fig. 1. Below T_N^{Tb}, however, only the q-FM mode is observed in the $e_b h_a$ configuration (Fig. 2) that is in contrast to the $e_c h_a$ configuration (Fig. 1), where both AFMR modes are observed. The only difference between these two configurations is the direction of the electric field of light: $e||c$ in $e_c h_a$ while $e||b$ in $e_b h_a$. Thus, we conclude that it is electric field $e||c$ and not magnetic field $h||a$ of light that excites the q-AFM mode in the $e_c h_a$ configuration at $T<T_N^{Tb}$ proving that this mode gains electric-dipole activity below T_N^{Tb}. At the same time, the magnetic-dipole activity of q-AFM mode at $T<T_N^{Tb}$ is the same as at $T>T_N^{Tb}$, *i.e.* it remains in agreement with the selection rules listed in Table I. Indeed, in the Section 3.2.a we will show that the q-AFM mode is observed in the $e_b h_c$ configuration at $T = 1.5$ K $< T_N^{Tb}$ and H=0. Since the q-AFM mode is not active in $e||b$ (see Fig. 2), we deduce that it is $h||c$ that excites the mode. We also checked that the q-AFM mode is not observed in the $e_a h_b$ configuration at T=1.5 K, which excludes its $h||b$ activity. Thus, we conclude that the magnetic-dipole activity of q-AFM mode at $T<T_N^{Tb}$ is $h||c$, in agreement with Table I. As for the q-FM mode, it was observed in all possible Faraday configurations below T_N^{Tb} which does not allow us to separate its pure magnetic-dipole activity from any possible electric-dipole contribution.

The line, which appears at 27 cm^{-1} in the $e_c h_a$ configuration in the narrow temperature region $T_{SR2}<T<T_N^{Tb}$ (see Fig. 1), was observed only in the $e||c$ configurations. For example, it was also observed at $T_{SR2}<T<T_N^{Tb}$ in transmittance spectra measured in $e_c h_b$ configuration shown in Fig. 3. Since the activity of this excitation strongly depends on the orientation of Tb and Fe magnetic moments, we conclude that this mode is an electric-dipole active magnetic excitation, or an electromagnon. This mode is labeled correspondingly as EM in Figures 1 and 3.

While the AFMR modes are observed in the $e_c h_b$ configuration at $T<T_N^{Tb}$, no modes are observed just above T_N^{Tb} when Fe spins are in the $\Gamma_2(G_z F_x)$ state. This state of Fe allows for $h||(b,c)$ activity of the q-FM mode and one would expect it to be observed in Fig. 3 at $T>T_N^{Tb}$. Since this is not the case, we deduce that the frequency of the q-FM mode falls below the low-frequency cut-off of our measurements.

3.2 Magnon spectra in external magnetic fields

3.2.a *H||a*

Figures 4(a-c) and 4(d-f) show magnetic field dependence of transmittance spectra of $TbFeO_3$ measured for $H||a$ at different temperatures in the $e_b h_c$ and $e_c h_b$ configurations,

correspondingly. At T=1.5 K and zero field the q-FM and q-AFM modes are observed simultaneously in both configurations at 24 cm^{-1} and 26 cm^{-1}, respectively [see Figs. 4(a,d)]. With the field increase along the a axis Fe spins enter into an angular Γ_{42} ($G_{xz}F_{zx}$) phase in which the ferromagnetic vector $\boldsymbol{F}$ rotates from the c-axis towards the a-axis while the antiferromagnetic vector $\boldsymbol{G}$ rotates from the a axis towards c [8,12,14]. At $\mu_0 H_{cr}^a = 1.3\,\mathrm{T}$ the q-FM mode hardens by 4 cm^{-1}, while the intensity of the q-AFM mode drops to zero. Earlier studies [8,12,14] showed that at H_{cr}^a Tb moments undergo metamagnetic transition $\Gamma_8(a_x g_y) \rightarrow \Gamma_2(f_x c_y)$ which finishes $\Gamma_{42}(G_{xz}F_{zx}) \rightarrow \Gamma_2(G_z F_x)$ reorientation of Fe spins. In the Γ_2 phase for Fe spins, the q-FM mode is active for $h||(b,c)$ and, thus, it can be observed both in the $e_b h_c$ and $e_c h_b$ configurations, as shown in Figs. 4(a,d) with a saturated frequency of ~28 cm^{-1} in high magnetic fields. At the same time, the q-AFM mode is $h||a$ active and, thus, is not observed in the $e_b h_c$ and $e_c h_b$ configurations in Figs. 4(a,d) for fields $H > H_{cr}^a$.

At temperatures $T_N^{Tb} < T < T_{SR1}$ and zero field, Fe spins undergo a continuous rotation from the Γ_4 (G_xF_z) phase, which is stable above T_{SR1}, to Γ_2 (G_zF_x), while Tb moments are in a paramagnetic state and are polarized by the effective field of Fe spins according to the Γ_2 (f_xc_y) irreducible representation. The application of magnetic field ~ 0.3 T along the a-axis completes the rotation of Fe spins from the a-axis towards c and stabilizes the Γ_2 (F_xG_z) structure of Fe spins [8,11,12]. Further increase of magnetic field increases the degree of Tb polarization until the latter reaches its saturation. Since the q-AFM mode is $h||a$ active in the Γ_2 (F_xG_z) state of Fe spins, this mode is not observed in our spectra measured in $e_b h_c$ and $e_c h_b$ configurations at $T_N^{Tb} < T < T_{SR1}$ shown in Figs. 4(b,e). Instead, the q-FM mode is $h||(b,c)$ active in the Γ_2 phase of Fe spins and, thus, one can expect it to be observed in Figs. 4(b,e). While the q-FM mode is indeed observed at fields above 1 T, it is not visible in magnetic fields below 1 T. We assume that in this case the frequency of the q-FM mode is below the lower edge of our measurements at 15 cm^{-1}. This result differs from the results of Raman measurements where the q-FM mode was reported to be at ≈18 cm^{-1} at $T_N^{Tb} < T < T_{SR1}$ and zero magnetic field [16]. With the field increase above 1 T the q-FM mode appears just above 15 cm^{-1} and its frequency gradually increases till it saturates at 28 cm^{-1}. Since magnetization of Fe subsystem gradually increases with the field increase but is far from saturation in the studied field range (0 - 8 T), it cannot contribute to the mechanism which leads to frequency saturation of the q-FM mode. Thus, we attribute the saturation of the q-FM mode to the saturation of Tb magnetization in the external magnetic field $H||a$.

At $T>T_{SR1}$ and H=0 the Fe spins are in the Γ_4 phase and Tb moments are paramagnetic. In this phase of Fe spins the q-FM mode is $h||(a,b)$ active and is observed in the $e_c h_b$

configuration at 17 cm^{-1} [see Fig. 4(f)], while the q-AFM mode is $h||c$ active and is observed in the e_bh_c configuration at 21 cm^{-1} [see Fig. 4(c)]. The application of magnetic field parallel to the a-axis results in reorientation of Fe spins from the Γ_4 (G_xF_z) phase to Γ_2 (F_xG_z) at $\mu_0 H_{cr}^a \approx 0.3$ T and polarizes the Tb system according to the Γ_2 (f_xc_y) configuration [8,12]. As in the case with the temperature region $T_N^{Tb} < T < T_{SR1}$ discussed above, only q-FM modes are observed in the final Γ_2 (F_xG_z) phase of Fe spins in both e_bh_c and e_ch_b configurations and its frequency gradually increases with the field increase till it saturates at 28 cm^{-1} in the field of 7 T [see Figs.4(c,f)] due to saturation of Tb moments. The saturation frequency of the q-FM mode is the same for all studied temperatures between 1.5 K to 11.8 K.

3.2.b *H*||*b*

Figures 5(a-b) show magnetic field dependence of transmittance measured for $H||b$ at T=1.5 K in the e_ch_a and e_ah_c configurations. Application of magnetic field along the b-axis results in a two-stage metamagnetic phase transition [10,12,14]. At T=1.5 K and zero field q-FM and q-AFM modes are observed simultaneously in both configurations at 24 cm^{-1} and 26 cm^{-1}, respectively [see Figs. 5(a,b)]. With the field increase along the b axis, Fe spins develop a ferromagnetic component F_y along the direction of magnetic field resulting in the Γ_{43} (G_xF_{zy}) magnetic structure. At the first critical field H_{cr1}^b magnetic moments of Tb^{3+} ions residing on one of the two sites, where Tb moments were opposite to the direction of the magnetic field, reorient towards the b axis. This reorientation results in the Γ_{8523} ($a_{xy}g_{yx}f_{xy}c_{yx}$) phase of Tb moments. This triggers reorientation of Fe spins from the a axis (Γ_{43}: G_xF_{zy}) to the c axis (Γ_{23}: G_zF_{xy}). The Γ_2 components of Fe magnetic structure allow for $h||a$ activity of the q-AFM mode and $h||(b,c)$ activity of the q-FM mode. For this reason in the Γ_{23} phase of Fe spins the q-AFM mode is observed in the e_ch_a configuration at 24−25 cm^{-1} [see Fig. 5(a)] and is not observed in e_ah_c one [Fig. 5(b)], while the q-FM mode is observed in the e_ah_c configuration at 16−17 cm^{-1} and is not observed in the e_ch_a one.

At the second critical field $\mu_0 H_{cr2}^b$=3 T magnetic moments of Tb^{3+} ions residing on the last site, where Tb moments were still opposite to the direction of the magnetic field, reorient towards the b axis, which results in the Γ_3 (f_yc_x) phase of Tb moments. This triggers reorientation of Fe spins back to the Γ_{43} (G_xF_{zy}) configuration. The Γ_4 components of Fe magnetic structure allow for $h||c$ activity of the q-AFM mode and $h||(a,b)$ activity of the q-FM mode. For this reason in the Γ_{43} phase of Fe spins the q-AFM mode is observed in the e_ah_c configuration at 21−23 cm^{-1} [see Fig. 5(b)] and is not observed in the e_ch_a configuration [Fig. 5(a)], while the q-FM mode is observed in the e_ch_a configuration at 15−16 cm^{-1} and is not observed in e_ah_c.

The behavior of magnetic modes throughout the course of two-stage magnetic phase transition is not trivial. Starting from zero field and up to $\mu_0 H^b_{cr1}$=0.7 T the q-AFM and q-FM modes are insensitive to the magnetic field. At H^b_{cr1} the q-AFM mode hardens by ~1 cm^{-1} [Fig.5(a)], while the q-FM mode drops from 24 cm^{-1} [Fig.5(a)] down to ~17 cm^{-1} [Fig.5(b)]. In the intermediate phase between H^b_{cr1} and H^b_{cr2} the q-AFM mode gradually softens from 27 cm^{-1} at H^b_{cr1} to 24 cm^{-1} at $\mu_0 H^b = 2.5$ T . Fig. 5(a) shows two events at $\mu_0 H^b = 2.5$ T . At first, the q-AFM mode frequency demonstrates a kink and then softens down to 23 cm^{-1}. Second, a new strong and broad mode appears at 30 cm^{-1} in a narrow field range of about 0.3 T. This mode has been confidently observed in 7 consecutive spectra measured with the field step of 0.05 T. In the Section 4.1 we will argue that this mode is related to the electromagnon EM mode observed at ≈27 cm^{-1} in transmittance spectra measured in $e_c h_a$ and $e_c h_b$ configurations in the narrow temperature range between T_{SR2} and T_N^{Tb} shown previously in Figs. 1 and 3. Above the H^b_{cr2} the q-AFM mode linearly softens from 23 cm^{-1} at H^b_{cr1} down to 21 cm^{-1} at 9 T.

Magnons' behavior in the temperature range $T_N^{Tb} < T < T_{SR1}$ and $H||b$ is presented in Fig. 6 for the $e_c h_a$ configuration and T=5.6 K. Earlier Mössbauer and magnetization studies showed that the application of magnetic field along the *b*-axis results in two successive metamagnetic phase transitions in Tb system and reorientation of Fe spins from the *c*-axis to the *a*-axis [6]. In zero field the Fe spins are close to the Γ_2 ($F_x G_z$) phase and polarize the paramagnetic Tb system according to the Γ_2 ($f_x c_y$) configuration. In this phase the q-AFM mode is $h||a$ active and is observed at 22 cm^{-1} (see Fig. 6). Application of a weak magnetic field along the *b*-axis results in a linear increase of the q-AFM mode's frequency. At $\mu_0 H^b_{cr1}$=1.7 T a spin reversal occurs on one of the Tb sites with an opposite direction of the moments relative to the field. With a further field increase the q-AFM mode frequency changes its slope sign and linearly decreases with the field. At $\mu_0 H^b_{cr2}$=4 T the second Tb spin reversal occurs and Tb spins become polarized according to the Γ_3 ($c_x f_y$) configuration. This triggers the movement of Fe spins from the *c*-axis towards *a*, where they are ordered in the Γ_{43} ($G_x F_{zy}$) phase. The Γ_4 components of Fe magnetic structure allows for $h||(a,b)$ activity of the q-FM mode and $h||c$ activity of the q-AFM mode. For this reason the q-AFM mode disappears above H^b_{cr2} in the $e_c h_a$ configuration giving way to the q-FM mode, which appears at 16 cm^{-1} (see Fig. 6). Aside from the AFMR modes no additional excitations, like the one at ≈30 cm^{-1} at T=1.5 K [see Fig. 5(a)], were observed at T=5.6 K or higher temperatures.

3.2.c *H*||*c*

At T=1.5 K application of magnetic field along the *c*-axis stabilizes $\Gamma_4(G_x F_z)$ structure of Fe spins and induces Tb polarization along the *c*-axis through the Van Vleck mechanism, while it

doesn't influence the splitting of the Tb ground quasi-doublet and Γ_8 (a_xg_y) arrangement of Tb moments [10,12,13]. Figure 7 shows magnetic field ($H||c$) dependence of the normalized transmittance measured in the e_ah_b configuration at T=1.5 K. A single mode is observed with a linear increase of the frequency from ≈23 cm^{-1} at H=0 to 27 cm^{-1} at $\mu_0 H = 5\,\mathrm{T}$. As it was discussed in Section 3.1, in the Γ_{48} ($G_xF_za_xg_y$) phase of $TbFeO_3$ the q-AFM mode is active only in (e,h)||c while the q-FM mode was observed in all configurations. Thus, it is the q-FM mode which is observed in the e_ah_b configuration at T=1.5 K (see Fig. 7). Its effective g-factor can be estimated from the slope of the linear dependence of the q-FM mode's frequency between 0 and 5 T: $g_{eff} = \Delta\omega_{FM} / \mu_B\mu_0\Delta H \approx 1.2$ where $\Delta\omega_{FM}$ is a frequency shift measured in [cm^{-1}] induced by a change of the magnetic field magnitude by $\mu_0\Delta H$, and μ_B is a Bohr magneton (μ_B ≈0.4669 cm^{-1}/T). We note, that the obtained value g_{eff}≈1.2 is about 40% smaller than the value g_{eff}≈2.1 obtained for $DyFeO_3$ in the same measurement conditions (T=1.5 K<T_N^{Dy}; $H||c$; Fe spins are in $\Gamma_4(G_xF_z)$ phase) [22].

IV. DISCUSSION

4.1 Electromagnon mode

As it was discussed in Section 3.1 a new EM mode appears at 27 cm^{-1} in the e_ch_a and e_ch_b configurations in the narrow temperature region $T_{SR2}<T<T_N^{Tb}$ bounded by two magnetic phase transitions [see Figs. 1(c) and Fig. 3]. The EM mode was observed only in the $e||c$ configurations and, thus, we attributed it to an electric dipole active magnetic excitation, or electromagnon. The appearance of the electromagnon mode at $T_{SR2}<T<T_N^{Tb}$ implies its relationship to the intermediate Γ_{28} ($G_zF_xa_xg_yf_xc_y$) phase in the sequence of the Tb magnetic ordering phases [4]. Interestingly, Γ_{28} phase allows for existence of spontaneous polarization $P||b$, while all other studied zero-field phases (Γ_{48} for $T<T_{SR2}$; Γ_2 for $T_N^{Tb}<T<T_{SR1}$; Γ_4 for $T>T_{SR1}$) are non-polar [48]. Spontaneous polarizations are also allowed in some of the phases induced by the magnetic field applied in the ab plane at $T<T_N^{Tb}$. Thus, the $P||a$ polarization can be induced by $H||a$ field in the Γ_{428} ($G_{xz}F_{zx}a_xg_y$; $0<H<H_{cr}^a$) phase and by $H||b$ field in the Γ_{438} ($G_xF_{zy}a_xg_y$; $0<H<H_{cr1}^b$) and Γ_{2358} ($G_zF_{xy}a_{xy}g_{yx}f_{xy}c_{yx}$) phases ($H_{cr1}^b<H<H_{cr2}^b$), while $P||b$ polarization can only be induced by $H||b$ in the intermediate Γ_{2358} ($G_zF_{xy}a_{xy}g_{yx}f_{xy}c_{yx}$) phase ($H_{cr1}^b<H<H_{cr2}^b$). Note that it was in the latter phase when the new excitation appeared at 30 cm^{-1} in the e_ch_a configuration at T=1.5 K in the external magnetic field $H||b$ [see Fig. 5(a)]. This excitation is positioned very close to the EM electromagnon observed at 27 cm^{-1} in Figs. 1 and 3 and they are both observed in the magnetic

phases which allow for spontaneous polarization P along the b axis. Thus, we deduce that the excitation at 30 cm^{-1} in Fig.5(a) is the same electromagnon mode EM which is observed in Figs.1 and 3. We can further contemplate that since the EM mode is polarized along the c-axis and is observed in the phases, which allow for static $P||b$ polarization, then the mode can be caused by oscillations of the $P||b$ polarization induced by the electric field of light $e \perp b$. Such explanation would account for $e||c$ dipole activity of this EM mode. Note that the existence of $P||b$ spontaneous polarization in $TbFeO_3$ crystals has not been experimentally confirmed yet. Thus, we are not able to make any affirmative conclusion about the exact mechanism of the EM excitation in $TbFeO_3$.

4.2 Quasi-FM mode in $H||a$

Application of magnetic field along the a-axis changes Fe and Tb magnetic structures so that their ferromagnetic components align along the field, which corresponds to the Γ_2 phases of Fe spins (G_zF_x) and Tb spins (f_xc_y). At $T<T_N^{Tb}$ the reorientation of Tb moments into the Γ_2 phase triggeres reorientation of Fe spins. These processes occur nearly simultaneously at $\mu_0 H_{cr}^a \sim 1.3$ T, which is accompanied by a sharp hardening of the q-FM mode by 4 cm^{-1} [Figs. 4(a,d)]. At $T>T_N^{Tb}$ the field-induced reorientation of Fe spins into the Γ_2 (G_zF_x) phase occurs in relatively low fields $\mu_0 H_{cr}^a \sim 0.3$ T, while the increase of polarization of paramagnetic Tb system in the $H||a$ field occurs gradually till it saturates at higher fields [11]. Figures 4(b,c,e,f) show that above H_{cr}^a the q-FM mode's frequency gradually increases with the field till it saturates at 28 cm^{-1}. Since magnetization of Fe system gradually increases with the field increase but is far from saturation in the studied field range, in Section 3.2.a we deduced that Fe magnetization cannot contribute to the mechanism which leads to frequency saturation of the q-FM mode and the latter is governed by the increase and saturation of the induced magnetization of paramagnetic Tb system. Below we will model magnetic field dependence of the q-FM mode's frequency for $H > H_{cr}^a$ and $T > T_N^{Tb}$. The ground state of Tb ions is an incidental quasi-doublet, which is separated from the excited states by $\sim 100\ cm^{-1}$ [49]. At low temperatures (< 20 K) only the quasi-doublet is populated and, thus, it governs the magnetic properties of Tb system. In this case the magnetic moments m_i (i=1,2,3,4) of the Tb sublattices along the corresponding Ising axes are:

$$m_i = \mu_{Tb} \tanh\left(\frac{\mu_{Tb}\mu_0 h_i}{kT}\right)$$

where $\mu_{Tb} \approx 8.6\mu_B$ [5] is a saturation value of Tb moments along the Ising axes, which is close to the maximum possible value of $9\mu_B$, and h_i is a magnetic field acting on Tb moments in the i^{th} position. In external magnetic field H_a acting along the a-axis we have [14]:

$$h_i = (H_a + aF_x + p'G_z)\cos\alpha + \sum_j T_{ij} m_j ,$$

where $a \approx 10$ T is the constant of the isotropic Tb−Fe interaction [4], $p' = 0.2959$ T is the constant of antisymmentric Tb−Fe dipole interaction [4] and T_{ij} are parameters of the Tb−Tb interaction, the values of which are given in Ref. [14]. The value of the weak cant of Fe moments in orthoferrites is $F_x \sim H_D/H_E \approx 0.01$, where $\mu_0 H_D \sim 10$ T is a Dzyaloshinskii field and $\mu_0 H_E \sim 10^3$ T is an exchange field [4]. It provides an estimate for the value of isotropic exchange field $\mu_0 a F_x \approx 0.1$ T. At $H > H_{cr}^a$ the Fe (as well as Tb) system is in the Γ_2 phase meaning that $G_z \approx 1$ and, thus, the value of the dipole field is $\mu_0 p' G_z \approx 0.3$ T. The Tb−Tb effective field reaches its maximum value at saturation of Tb moments. In Γ_2 phase ($H > H_{cr}^a$) this translates to $m_1 = m_2 = m_3 = m_4 = \mu_{Tb}$, which results in $\mu_0 \sum_j T_{ij} m_j = \mu_0 (T_{i1} + T_{i2} + T_{i3} + T_{i4}) \mu_{Tb} \approx 0.3$ T. The range of external fields $H \| a$, where the q-FM mode demonstrates hardening till it saturates at 28 cm^{-1}, is from ~1 to ~7 T (see Fig. 4). In this range the external field H_a provides the strongest contribution to h_i. Thus, we can neglect contributions coming from the Tb−Fe and Tb−Tb interactions in the first approximation. In this case the value of Tb magnetic momenets along the Ising axes in the Γ_2 phase can be estimated as:

$$m_{Tb} = \mu_{Tb} \tanh\left(\frac{\mu_{Tb}\mu_0 H_a}{kT}\right),$$

which is a function of H_a/T ratio. Figures 8(a,b) show magnetic field dependence of q-FM mode's frequency ploted as a function of $\mu_0 H_a / T$. The data obtained at different temperatures above $T_N^{Tb} = 3.3\,K$, *i.e.* when Tb moments are paramagnetic, nicely overlap. This indicates that q-FM mode's frequency depends only on $\mu_0 H_a / T$, rather than separately on H_a and T, just as m_{Tb} does. For this reason we modeled data from Figs. 8(a,b) assuming a linear dependence between the q-FM mode's frequency and Tb magnetization: $\omega_{FM} = \omega_{FM,\max} \tanh\left(\frac{\mu_{Tb}\mu_0 H_{ext}}{kT}\right)$, where $\omega_{FM,\max} = 28.3\,\text{cm}^{-1}$ is a saturation frequency of the q-FM mode at high magnetic fields. The results of the modeling are in good agreement with the experimental data providing we use the value $\mu_{Tb} = 7.2\mu_B$ which is smaller than experimentally reported value $\mu_{Tb} = 8.6\mu_B$ [5]. This difference can be due to contributions from Tb−Fe and Tb−Tb interactions to the effective magnetic field acting on Tb moments, which we neglected in our simplified model. For a more precise fit these interactions should be taken into account.

Figure 8 shows that frequency of the q-FM mode at zero magnetic field extrapolates to zero, which does not need to be the case if all interactions are taken into account. For $T > T_{SR1}$ as we reduce the field, the $\Gamma_2 \rightarrow \Gamma_4$ reorientation of Fe spins takes place and q-FM mode's frequency

shifts to 17 cm^{-1}. For $T_N^{Tb} < T < T_{SR1}$ as we reduce the field, we cannot neglect the effective field created by Tb−Fe interaction which does not go to zero when external field goes to zero. Also, as the frequency of the q-FM mode lowers we might need to take into account interaction with the lower lying Tb quasi-doublet, which is split by the Tb−Fe interaction and external field. Nevertheless, our data imply that the frequency of the q-FM mode seems to be at least below 15 cm^{-1} in the Γ_2 phase of Fe spins and zero external field.

4.3 Comparison between magnon and electromagnon spectra of $TbFeO_3$ and $DyFeO_3$

Recently we reported studies of magnon and electromagnon excitations in another member of the rare-earth orthoferrites family, namely $DyFeO_3$ [22]. From the first glance, $TbFeO_3$ and $DyFeO_3$ are very similar and their difference is only due to one *f*-electron at the R^{3+} sites. Both Tb and Dy ions have similar anisotropies of the ground state in these compounds: the ground state of Tb ions is incidental quasi-doublet with Ising axes lying in the *a*−*b* plane at $\pm 36^\circ$ to the *a*-axis and the ground state of Dy ions is a Kramer's doublet which can be interpreted as a close to $|\pm 15/2\rangle$ state with axes of quantization lying in the *a*−*b* plane at $\pm 60^\circ$ to the *a*-axis. The rare-earth ions in both compounds antiferromagnetically order in the *a*−*b* plane at temperatures between 3 and 4 K and manifest close values of saturated magnetic moments: $\mu_{Tb} \approx 8.6\mu_B$ [5] and $\mu_{Dy} \approx 9.2\mu_B$ [50]. In both cases rare-earth ordering results in hardening of AFMR modes and appearance of electromagnon modes which are optically active for *e*||*c*.

Despite seeming similarity, the properties of Tb and Dy orthoferrites are quite different. $DyFeO_3$ is the only representative of orthoferrites family which manifests Morin type reorientation of Fe spins from the *a*-axis (Γ_4 phase) to the *b*-axis (Γ_1 phase). This transition is driven by Dy-Fe interaction which lowers the energy of the Dy ground doublet (without splitting it) via the Van-Vleck mechanism which mixes Dy ground state with excited states [51]. The energy shift is bigger when Fe spins are directed along the *b*-axis competing with the intrinsic anisotropy of the Fe system which prefers the a-axis. As temperature lowers, the Dy ground state becomes more populated which increases the anisotropy of Dy system and, hence, reduces the overall anisotropy in the *a*−*b* plane resulting in a reduction of K_{ab} anisotropy constant of thermodynamic potential [51]. As a result, the q-AFM mode, which is determined by the K_{ab} anisotropy constant becomes a soft mode of the transition [52]. When anisotropy constant K_{ab} changes sign, reorientation of Fe spins from the *a*-axis to the *b*-axis takes place.

In contrast, $TbFeO_3$, like most rare-earth orthoferrites, manifests continuous $\Gamma_4 \rightarrow \Gamma_2$ spin reorientation transition during which Fe spins rotate from the *a*-axis to the *c*-axis. This transition is driven by lowering of energy of Tb system due to splitting of the ground Tb quasi-doublet by the effective field created by the Tb−Fe interaction. Such splitting takes place only when antiferromagnetic vector ***G*** of Fe spins leaves the *a*−*b* plane. As temperature lowers, the lower level of the split quasi-doublet becomes more populated than the upper one which

increases the anisotropy of the Tb system and reduces the overall anisotropy in the $a-c$ plane resulting in a reduction of the K_{ac} anisotropy constant [4]. As a result, the q-FM mode, which is determined by K_{ac} [18], should become a soft mode of the transition. Earlier Raman measurements of AFMR modes showed [16] that this was not the case and the q-FM mode's frequency stayed at ≈18 cm^{-1} throughout the course of $\Gamma_4 \rightarrow \Gamma_2$ spin reorientation transition. It was suggested [16,18] that interaction of the q-FM mode with the lower-lying Tb quasi-doublet might be responsible for this. In our study we didn't observe softening of the q-FM mode down to the spin-reorientation temperature T_{SR1}=8.5 K (see Fig. 1). Between T_{SR1} and T_N^{Tb} we were not able to track the q-FM mode probably because its intensity dropped to zero or because its frequency dropped below the lower cut-off of our measurements, which is 15 cm^{-1}. The latter seems more plausible taking into account that the extrapolated position of the q-FM mode when Fe spins are in Γ_2 phase and external magnetic field goes to zero is below 15 cm^{-1} [See Figs. 4(b,e) and 8].

The electromagnon spectra in $TbFeO_3$, which appear below the temperature of rare-earth ordering, also significantly differ from that in $DyFeO_3$. In $DyFeO_3$ we have not found any electric dipole activity of the AFMR modes while in $TbFeO_3$ the q-AFM mode gained electric dipole activity along the c-axis below T_N^{Tb} and became a hybrid mode. In $DyFeO_3$ there are two electromagnon modes at ~20 and ~50 cm^{-1}, which appear in the non-polar Γ_{15} phase. In $TbFeO_3$ there seems to be only one electromagnon EM mode (different from the q-AFM mode) at ~27 cm^{-1}, which appears in phases compatible with spontaneous electric polarization along the b-axis. Electromagnons seem to be more stable and strong in $DyFeO_3$, where they exist in the whole temperature range $T < T_N^{Dy} = 4.2$ K. In $DyFeO_3$ we were able to relate the electromagnon mode at ~20 cm^{-1} to the field-induced variation and hysteresis of the dielectric constant [22]. In contrast, the electromagnon EM in $TbFeO_3$ is much weaker and it appears only in a very narrow range of temperatures (2.7 K < T < T_N^{Tb}=3.3 K) and fields (2.4 - 2.7 T; $H||b$) making its observation in optical spectra quite challenging.

V. CONCLUSSION.

The temperature and magnetic-field dependencies of the AFMR spectra have been measured below and above the magnetic ordering of Tb moments T_N^{Tb}≈3.3 K. Both quasi-ferromagnetic and quasi-antiferromagnetic modes of AFMR demonstrate hardening at $T<T_N^{Tb}$. The quasi-antiferromagnetic mode gains electric-dipole activity along the c axis below T_N^{Tb} and becomes a hybrid mode. In addition to the AFMR modes, we have reported an observation of electromagnon mode, which is electric-dipole active along the c axis and appears at ~27 cm^{-1} in

the narrow temperature region 2.7 K < T < T_N^{Tb} at H=0 and at ~30 cm^{-1} in the narrow range of magnetic fields 2.4 T < $\mu_0 H_b$ < 2.7 T applied along the b-axis at T=1.5 K. This electromagnon appears in magnetic phases, which are compatible with spontaneous electric polarization along the b-axis.

ACKNOWLEDGMENTS

The authors are grateful to G. L. Carr for help with the measurements at U4-IR beamline of NSLS and to S. Artyukhin, M. Mostovoy, and A. Mukhin for their interest and useful discussions. Work at the New Jersey Institute of Technology and Rutgers University was supported by the U.S. Department of Energy under Contract No. DEFG02-07ER46382. Use of the National Synchrotron Light Source, Brookhaven National Laboratory, was supported by the U.S. Department of Energy under Contract No. DE-AC02- 98CH10886.

Table I. Selection rules for quasi-ferromagnetic (q-FM) and quasi-antiferromagnetic (q-AFM) modes of AFMR in RFeO$_3$. [18, 47]

Fe phase	q-FM		q-AFM	
	Oscillation quantities	Activity	Oscillation quantities	Activity
$\Gamma_1(G_y)$	G_zF_x	$h\|\|a$	G_xF_z	$h\|\|c$
$\Gamma_2(G_zF_x)$	$F_yF_zG_x$	$h\|\|b$, $h\|\|c$	$G_yF_xG_z$	$h\|\|a$
$\Gamma_4(G_xF_z)$	$G_zF_xF_y$	$h\|\|a$, $h\|\|b$	$G_yG_xF_z$	$h\|\|c$

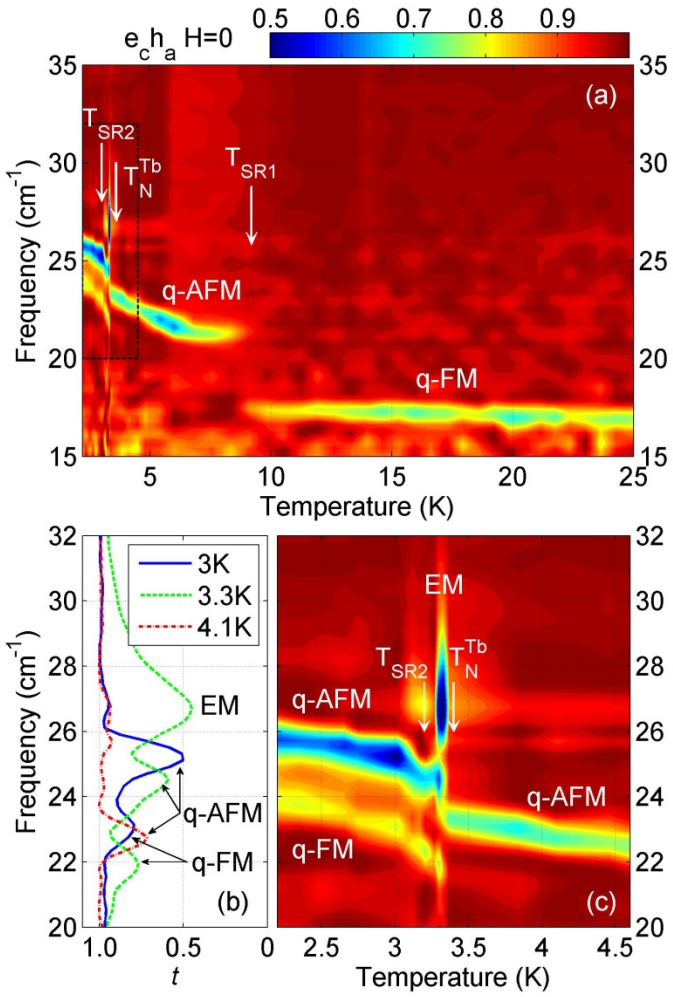

FIG. 1. (Color online) (a) Normalized transmittance map of TbFeO$_3$ measured in the e_ch_a configuration at temperatures from 2 to 25 K. (b) Spectra of transmittance t for temperatures above (4.1 K), at (3.3 K) and below (3 K) the temperature of Tb magnetic ordering T_N^{Tb}≈3.3 K. (c) An expanded view of the rectangular region in (a) showing the behavior of q-AFM, q-FM, and EM excitations in the vicinity of Tb magnetic ordering.

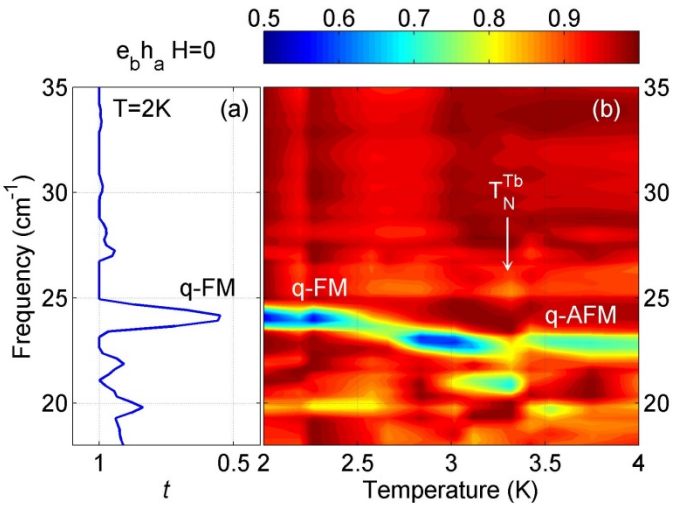

FIG. 2. (Color online) (a) Normalized transmittance spectrum t of $TbFeO_3$ measured in the $e_b h_a$ configuration at T=2 K<T_N^{Tb} and H=0. (b) Normalized transmittance map manifesting q-FM excitation below T_N^{Tb} and q-AFM one above T_N^{Tb}.

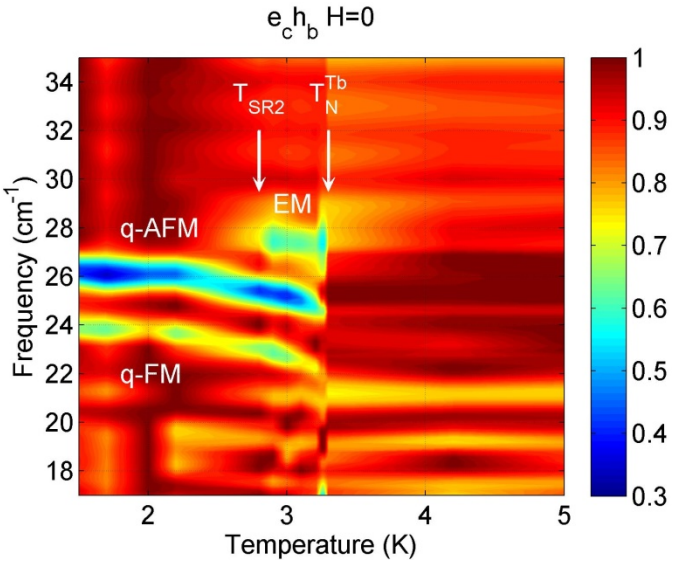

FIG. 3. (Color online) Temperature dependence of the normalized transmittance of $TbFeO_3$ measured in the $e_c h_b$ configuration at H=0 manifesting q-AFM, q-FM, and EM excitations below T_N^{Tb}. Electromagnon EM is visible in a narrow temperature region between T_{SR2} and T_N^{Tb}.

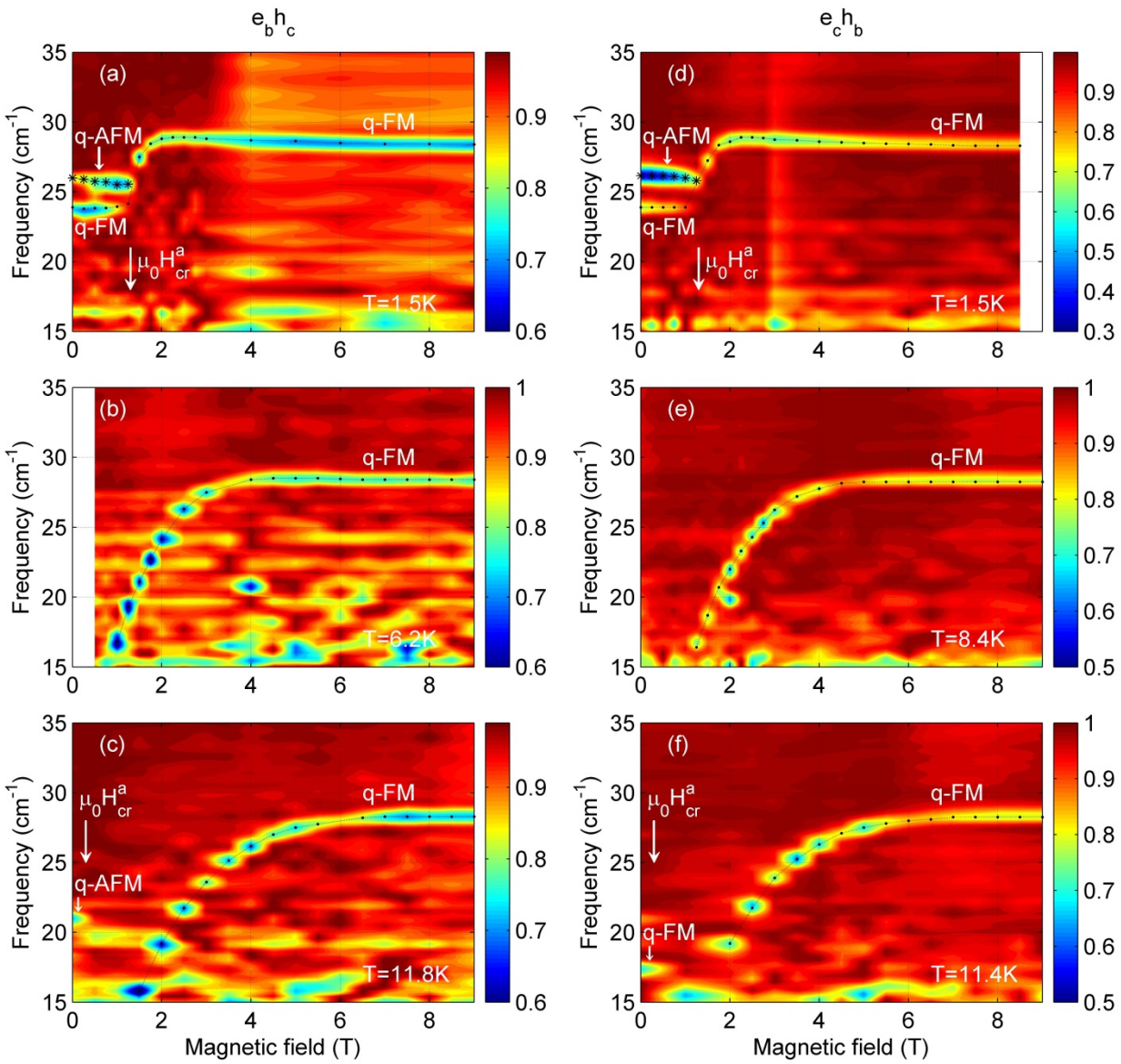

FIG. 4. (Color online). Magnetic field dependence ($H||a$) of normalized transmittance measured in the $e_b h_c$ configuration at (a) 1.5 K, (b) 6.2 K and (c) 11.8 K and in the $e_c h_b$ configuration at (d) 1.5 K, (e) 8.4 K and (f) 11.4 K.

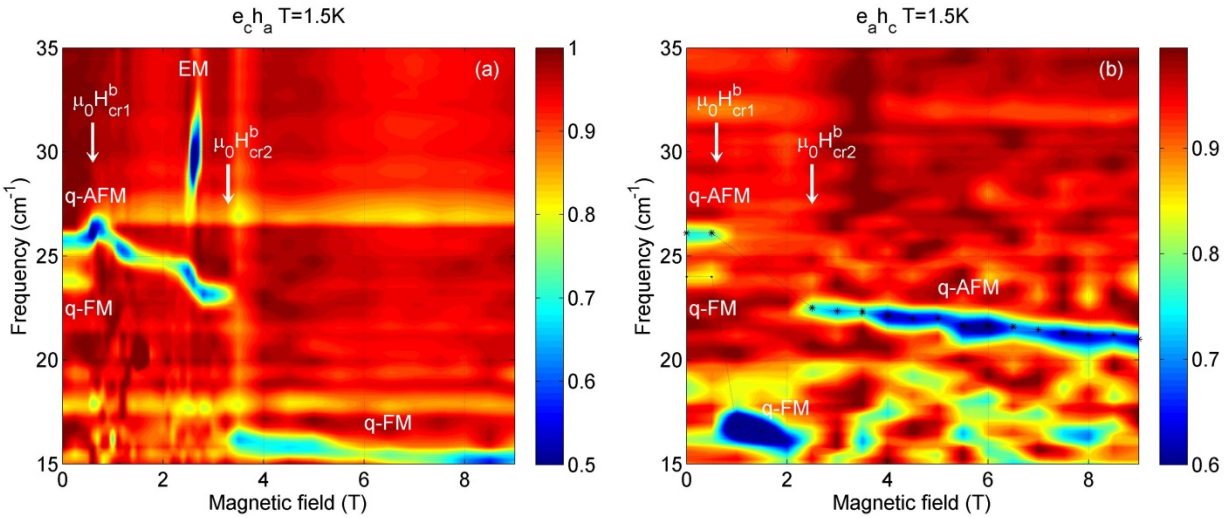

FIG. 5. (Color online) Magnetic field dependence ($H||b$) of normalized transmittance measured in the e_ch_a (a) and e_ah_c (b) configurations at T=1.5 K

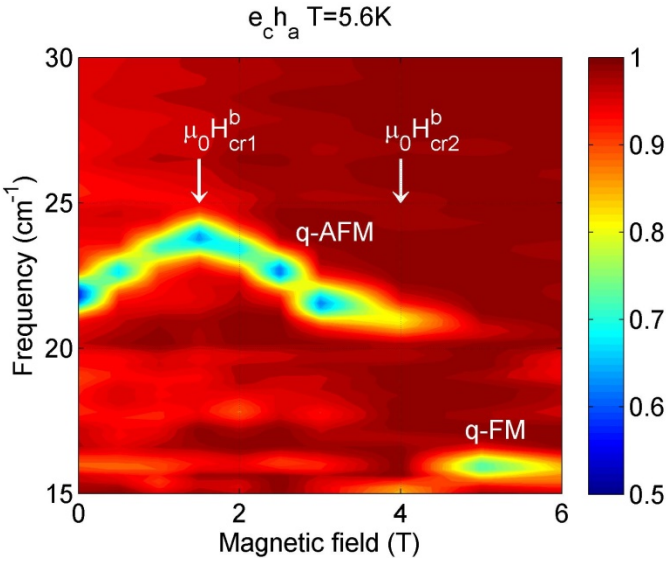

FIG. 6. (Color online) Magnetic field dependence ($H||b$) of normalized transmittance spectra measured in the e_ch_a configuration at T=5.6 K.

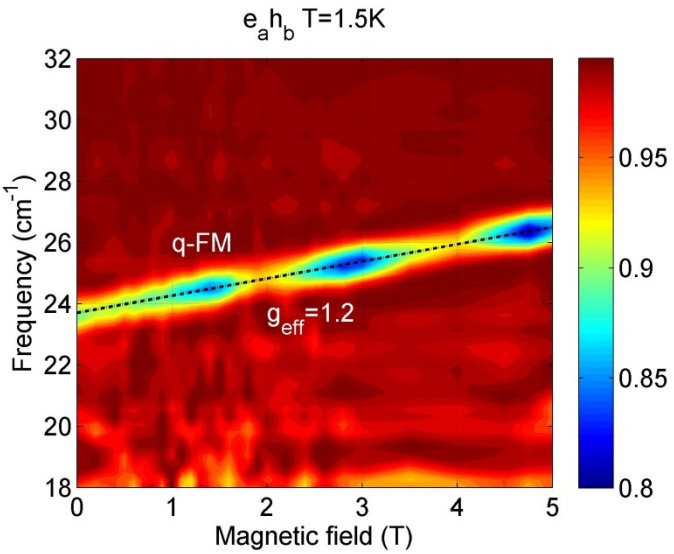

FIG. 7. (Color online) Magnetic field dependence ($H||c$) of normalized transmittance measured in the $e_a h_b$ configuration at T=1.5 K.

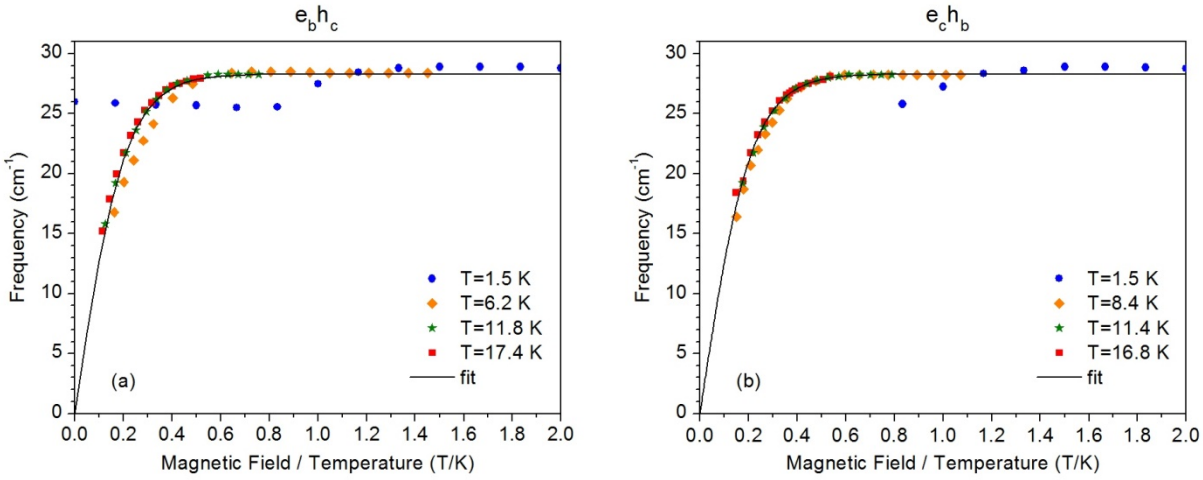

FIG. 8. (Color online) Experimental data for the q-FM mode's frequency measured in the $e_b h_c$ (a) and $e_c h_b$ (b) configurations in the magnetic field $H||a$ presented as a function of $\mu_0 H_a / T$.

REFERENCES

[1] S. Geller and E. A. Wood, *Crystallographic studies of perovskite-like compounds. I. Rare earth orthoferrites and $YFeO_3$, $YCrO_3$, $YAlO_3$*, Acta Cryst. **9**, 563-568 (1956).

[2] M. Marezio, J. P. Remeika and P. D. Dernier, *The Crystal Chemistry of Rare Earth Orthoferrites*, Acta Cryst. B **26**, 2008 (1970).

[3] R. L. White, *Review of Recent Work on the Magnetic and Spectroscopic Properties of the Rare-Earth Orthoferrites*, J. Appl. Phys. **40**, 1061 (1969).

[4] K. P. Belov, A. K. Zvezdin, and A. A. Mukhin, *Magnetic phase transitions in terbium orthoferrite*, Sov. Phys. JETP **49** (3), 557 (1979).

[5] E. F. Bertaut, J. Chappert, J. Mareschal, J. P. Rebouillat and J. Sivardiere, *Structures Magnetiques de $TbFeO_3$*, Solid State Commun. **5**, 293 (1967).

[6] O. Nikolov, I. Hall, S. N. Barilo and S. A. Guretskii, *A Mossbauer study of temperature-driven spin-reorientation transitions in $TbFeO_3$*, J. Phys.: Condens. Matter **6**, 3793 (1994).

[7] J. Mareschal, J. Sivardière, G. F. De Vries and E. F. Bertaut, *Magnetic Ordering of Terbium in Some Perovskite Compounds*, J. Appl. Phys. **39**, 1364 (1968).

[8] S. A. Guretskii, A. P. Ges, A. M. Luginets, A. S. Milovanov, V. D. Fil', S. V. Zherlitsyn, *Low-temperature Magnetic Properties of Terbium Orthoferrite Single Crystals*, Cryst. Res. Technol. **31**, 897 (1996).

[9] V. N. Derkachenko, A. K. Zvezdin, I. B. Krynetskii, A. M. Kadomtzeva, A. A. Mukhin, and V. A. Khokhlov, *Magnetic-field induced spin-reorientation phase-transitions in terbium ortho-ferrite*, Fiz. Tv. Tela **22**, 1753 (1980) [Sov. Phys.-Solid State **22**, 1021 (1980)].

[10] J.E. Bourée and J. Hammann, *Mise en évidence expérimentale des effets de forme dans l'orthoferrite de terbium*, J. Phys. France **36**, 391 (1975).

[11] O. Nikolov, I. Hall, S. N. Barilo, and A. A. Mukhin, *Field-induced spin reorientations in $TbFeO_3$ at 4.2 K*, J. Magn. Magn. Mater. **152**, 75 (1996).

[12] Yiming Cao, Maolin Xiang, Weiyao Zhao, Guohua Wang, Zhenjie Feng, Baojuan Kang, Alessandro Stroppa, Jincang Zhang, Wei Ren, and Shixun Cao, *Magnetic phase transition and*

giant anisotropic magnetic entropy change in $TbFeO_3$ single crystal, J. Appl. Phys. **119**, 063904 (2016).

[13] S. Artyukhin, M. Mostovoy, N. P. Jensen, D. Le, K. Prokes, V. G. Paula, H. N. Bordallo, A. Maljuk, S. Landsgesell, H. Ryll, B. Klemke, S. Paeckel, K. Kiefer, K. Lefmann, L. T. Kuhn, and D. N. Argyriou, *Solitonic lattice and Yukawa forces in the rare earth orthoferrite $TbFeO_3$*, Nat. mater. **11** (8), 694 (2012).

[14] K. P. Belov, A. K. Zvezdin, A. M. Kadomtseva, N. B. Krynetskii, and A. A. Mukhin, *Metamagnetic phase transitions and instability of magnetic structure in rare-earth orthoferrites*, Sov. Phys. JETP **49**, 723 (1979).

[15] A. Gukasov, U. Steinenberger, S. N. Barilo, and S. A. Guretskii, *Neutron scattering study of spin waves in $TbFeO_3$*, Physica B **234-236**, 760 (1997).

[16] S. Venugopalan, M. Dutta, A. K. Ramdas, and J. P. Remeika, *Raman scattering study of magnons at the spin-reorientation transitions of $TbFeO_3$ and $TmFeO_3$*, Phys. Rev. B **27**, 3115 (1983).

[17] S. Venugopalan, M. Dutta, A. K. Ramdas, and J. P. Remeika, *Magnetic and vibrational excitations in rare-earth orthoferrites: A Raman scattering study*, Phys. Rev. B **31**, 1491 (1985).

[18] A.M. Balbashov, G.V. Kozlov, A.A. Mukhin, A.S. Prokhorov, *Submillimeter spectroscopy of antiferromagnetic dielectrics: rare-earth orthoferrites*, in High Frequency Processes in Magnetic Materials, edited by G. Srinivasan, A. Slavin (World Scientific, Singapore, 1995), Part I, pp. 56–98.

[19] S.M. Shapiro, J.D. Axe and J.P. Remeika, *Neutron-scattering studies of spin waves in rare-earth orthoferrites*, Phys. Rev. B **10**, 2014-2021 (1974).

[20] N. Koshizuka and S. Ushioda, *Inelastic-light-scattering study of magnon softening in $ErFeO_3$*, Phys. Rev. B **22**, 5394 (1980).

[21] R. M. White, R. J. Nemanich, and Conyers Herring, *Light scattering from magnetic excitations in orthoferrites*, Phys. Rev. B **25**, 1822 (1982).

[22] T. N. Stanislavchuk, Yazhong Wang, Y. Janssen, G. L. Carr, S.-W. Cheong, and A. A. Sirenko, *Magnon and electromagnon excitations in multiferroic $DyFeO_3$*, Phys. Rev. B **93**, 094403 (2016).

[23] K. B. Aring and A. J. Sievers, *Role of the Ytterbium Spins in the Spin Reorientation in $YbFeO_3$*, J. Appl. Phys. **41**, 1197 (1970).

[24] R. C. LeCraw, R. Wolfe, E. M. Gyorgy, F. B. Hagedorn, J. C. Hensel, and J. P. Remeika, *Microwave Absorption near the Reorientation Temperature in Rare Earth Orthoferrites*, J. Appl. Phys. **39**, 1019 (1968).

[25] A. V. Kimel, C. D. Stanciu, P. A. Usachev, R. V. Pisarev, V. N. Gridnev, A. Kirilyuk, and Th. Rasing, *Optical excitation of antiferromagnetic resonance in $TmFeO_3$*, Phys. Rev. B **74**, 060403(R) (2006).

[26] V. G. Bar'yakhtar and I. E. Chupis, *Quantum theory of oscillations in a ferroelectric ferromagnet*, Sov. Phys. Solid State **11**, 2628 (1970).

[27] A. Pimenov, A. A. Mukhin, V. Yu. Ivanov, V. D. Travkin, A. M. Balbashov, and A. Loidl, *Possible evidence for electromagnons in multiferroic manganites*, Nat. Phys. **2**, 97 (2006).

[28] V. N. Krivoruchko, *Electrically active magnetic excitations in antiferromagnets (Review Article)*, Low Temp. Phys. **38**, 807 (2012).

[29] S. Dong, J.-M. Liu, S.-W. Cheong and Z. Ren, *Multiferroic materials and magnetoelectric physics: symmetry, entanglement, excitation, and topology*, Adv. Phys. **64**, 519 (2015).

[30] Y. Tokura, S. Seki and N. Nagaosa, *Multiferroics of spin origin*, Rep. Prog. Phys. **77**, 076501 (2014).

[31] I. Kézsmárki, N. Kida, H. Murakawa, S. Bordács, Y. Onose, Y. Tokura, *Enhanced Directional Dichroism of Terahertz Light in Resonance with Magnetic Excitations of the Multiferroic $Ba_2CoGe_2O_7$ Oxide Compound*, Phys. Rev. Lett. **106**, 057403 (2011).

[32] David Szaller, Sandor Bordacs, and Istvan Kezsmarki, *Symmetry conditions for nonreciprocal light propagation in magnetic crystals*, Phys. Rev. B **87**, 014421 (2013).

[33] A. M. Kuzmenko, A. Shuvaev, V. Dziom, Anna Pimenov, M. Schiebl, A. A. Mukhin, V. Yu. Ivanov, L. N. Bezmaternykh, and A. Pimenov, *Giant gigahertz optical activity in multiferroic ferroborate*, Phys. Rev. B **89**, 174407 (2014).

[34] I. Kézsmárki, U. Nagel, S. Bordács, R. S. Fishman, J. H. Lee, Hee Taek Yi, S.-W. Cheong, and T. Rõõm, *Optical Diode Effect at Spin-Wave Excitations of the Room-Temperature Multiferroic $BiFeO_3$*, Phys. Rev. Lett. **115**, 127203 (2015).

[35] T. Kubacka, J. A. Johnson, M. C. Hoffmann, C. Vicario et al, *Large-Amplitude Spin Dynamics Driven by a THz Pulse in Resonance with an Electromagnon*, Science **343**, 1333 (2014).

[36] R. Valdes Aguilar, M. Mostovoy, A. B. Sushkov, C. L. Zhang, Y. J. Choi, S-W. Cheong, and H. D. Drew, *Origin of Electromagnon Excitations in Multiferroic $RMnO_3$*, Phys. Rev. Lett. **102**, 047203 (2009).

[37] H. Katsura, A.V. Balatsky and N. Nagaosa, *Dynamical Magnetoelectric Coupling in Helical Magnets*, Phys. Rev. Lett. **98**, 027203 (2007).

[38] T. Nakajima, A. Suno, S. Mitsuda, N. Terada, S. Kimura, K. Kaneko and H. Yamauchi, *Magnons and electromagnons in a spin-lattice-coupled frustrated magnet $CuFeO_2$ as seen via inelastic neutron scattering*, Phys. Rev. B **84**, 184401 (2011).

[39] I.A. Sergienko, C. Sen and E. Dagotto, *Ferroelectricity in the Magnetic E-Phase of Orthorhombic Perovskites*, Phys. Rev. Lett. **97**, 227204 (2006).

[40] I.A. Sergienko and E. Dagotto, *Role of the Dzyaloshinskii-Moriya interaction in multiferroic perovskites*, Phys. Rev. B **73**, 094434 (2006).

[41] M. Mostovoy, *Ferroelectricity in spiral magnets*, Phys. Rev. Lett. **96**, 067601 (2006).

[42] H. Katsura, N. Nagaosa and A.V. Balatsky, *Spin Current and Magnetoelectric Effect in Noncollinear Magnets*, Phys. Rev. Lett. **95**, 057205 (2005).

[43] T. Arima, *Ferroelectricity Induced by Proper-Screw Type Magnetic Order*, J. Phys. Soc. Jpn. **76**, 073702 (2007).

[44] H.C. Walker, F. Fabrizi, L. Paolasini, F. de Bergevin, J. Herrero-Martin, A.T. Boothroyd, D. Prabhakaran and D.F. McMorrow, *Femtoscale Magnetically Induced Lattice Distortions in Multiferroic $TbMnO_3$*, Science **333**, 1273 (2011).

[45] N. Kida, D. Okuyama, S. Ishiwata, Y. Taguchi, R. Shimano, K. Iwasa, T. Arima and Y. Tokura, *Electric-dipole-active magnetic resonance in the conical-spin magnet $Ba_2Mg_2Fe_{12}O_{22}$*, Phys. Rev. B **80**, 220406 (2009).

[46] D. A. Yablonskii and V. N. Krivoruchko, *Antiferroelectric resonance in rare-earth orthoferrites*, Sov. Phys. Solid State **30**, 1765 (1988).

[47] V. G. Bar'yakhtar, I. M. Vitebskii, and D. A. Yablonskii, *Symmetry and magnetic-resonance frequencies in magnetically ordered crystals*, Sov. Phys. JETP **49**, 703 (1979).

[48] A. K. Zvezdin and A. A. Mukhin, *Magnetoelectric Interactions and Phase Transitions in a New Class of Multiferroics with Improper Electric Polarization*, JETP Letters **88**, 505 (2008).

[49] J. Rossat-Mignod and F. Tcheou, *Effet du champ cristallin sur la direction des moments magnétiques des ions de terres rares occupant des sites de très basse symétrie* (C_2-Cs), J. Phys. (Paris) **33**, 423 (1972).

[50] G. Gorodetsky, B. Sharon, and S. Shtrikman, *Magnetic Properties of an Antiferromagnetic Orthoferrite*, J. Appl. Phys. **39**, 1371 (1968).

[51] A. K. Zvezdin and V. M. Matveev, *Theory of the magnetic properties of dysprosium orthoferrite*, Sov. Phys. JETP **77**, 1076 (1979).

[52] A. M. Balbashov, A. A. Volkov, S. P. Lebedev, A. A. Mukhin, and A. S. Prokhorov, *High-frequency magnetic properties of dysprosium orthoferrite*, Sov. Phys. JETP **61**, 573 (1985).